

AD-A238 052



2

NAVAL POSTGRADUATE SCHOOL

Monterey, California



DTIC
ELECTE
JUL 12 1991
S B D

THESIS

Effect of Alumina Particle Additions on the Aging Kinetics
of 6061 Aluminum Matrix Composites

by

Susan Marie Allen

June, 1990

Thesis Advisor:

I. Dutta

Approved for public release; distribution is unlimited.

65 91-04491



91 7 09 065

REPORT DOCUMENTATION PAGE

Form Approved
OMB No 0704-0188

1a REPORT SECURITY CLASSIFICATION UNCLASSIFIED		1b RESTRICTIVE MARKINGS	
2a SECURITY CLASSIFICATION AUTHORITY		3 DISTRIBUTION / AVAILABILITY OF REPORT Approved for public release: distribution is unlimited.	
2b DECLASSIFICATION / DOWNGRADING SCHEDULE		4 PERFORMING ORGANIZATION REPORT NUMBER(S)	
4 PERFORMING ORGANIZATION REPORT NUMBER(S)		5 MONITORING ORGANIZATION REPORT NUMBER(S)	
6a NAME OF PERFORMING ORGANIZATION Naval Postgraduate School	6b OFFICE SYMBOL (If applicable) Code 69	7a NAME OF MONITORING ORGANIZATION	
6c ADDRESS (City, State, and ZIP Code) Monterey, California 93943-5000		7b ADDRESS (City, State, and ZIP Code)	
8a NAME OF FUNDING / SPONSORING ORGANIZATION	8b OFFICE SYMBOL (If applicable)	9 PROCUREMENT INSTRUMENT IDENTIFICATION NUMBER	
8c ADDRESS (City, State, and ZIP Code)		10 SOURCE OF FUNDING NUMBERS	
		PROGRAM ELEMENT NO	PROJECT NO
		TASK NO	WORK UNIT ACCESSION NO
11 TITLE (Include Security Classification) EFFECT OF ALUMINA PARTICLE ADDITIONS ON THE AGING KINETICS OF 6061 ALUMINUM MATRIX COMPOSITES (UNCLAS)			
12 PERSONAL AUTHOR(S) Susan M. Allen			
13a TYPE OF REPORT	13b TIME COVERED FROM _____ TO _____	14 DATE OF REPORT (Year, Month, Day) June 1990	15 PAGE COUNT 64
16 SUPPLEMENTARY NOTATION The views expressed in this thesis are those of the author and do not reflect the official policy of the Department of Defense or the U.S. Government.			
17 COSATI CODES		18 SUBJECT TERMS (Continue on reverse if necessary and identify by block number)	
FIELD	GROUP	SUB-GROUP	
		Aluminum Matrix Composites	
19 ABSTRACT (Continue on reverse if necessary and identify by block number)			
<p>Differential scanning calorimetry (DSC) was conducted using a monolithic 6061 aluminum material and two 6061 aluminum matrix composite materials. The composite materials were reinforced with 10 volume percent and 15 volume percent alumina particles. Electrical resistivity and hardness measurements during isothermal aging treatments were also conducted. The effects of prior aging and alumina particle additions on the growth kinetics and the thermal stability of the metastable phases in each material were studied. The results were used to characterize the effect of reinforcement on the aging kinetics of composite materials.</p>			
20 DISTRIBUTION / AVAILABILITY OF ABSTRACT <input checked="" type="checkbox"/> UNCLASSIFIED/UNLIMITED <input type="checkbox"/> SAME AS RPT <input type="checkbox"/> DTIC USERS		21 ABSTRACT SECURITY CLASSIFICATION Unclassified	
22a NAME OF RESPONSIBLE INDIVIDUAL I. Dutta, Professor		22b TELEPHONE (Include Area Code) (408) 646-2581	22c OFFICE SYMBOL 69DU

Approved for public release; distribution is unlimited.

**Effect of Alumina Particle Additions on the Aging Kinetics
of 6061 Aluminum Matrix Composites**

by

Susan Marie Allen
Lieutenant Commander, United States Navy
B.S., University of Rochester, 1979

Submitted in partial fulfillment
of the requirements for the degree of

MASTER OF SCIENCE IN MECHANICAL ENGINEERING

from the

NAVAL POSTGRADUATE SCHOOL


June 1990

Author:

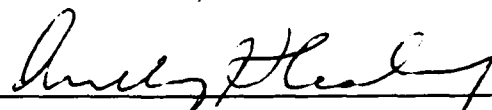


Susan Marie Allen

Approved by:



I. Dutta, Thesis Advisor



Anthony Healey, Chairman
Department of Mechanical Engineering

ABSTRACT

Differential scanning calorimetry (DSC) was conducted using a monolithic 6061 aluminum material and two 6061 aluminum matrix composite materials. The composite materials were reinforced with 10 volume percent and 15 volume percent alumina particles. Electrical resistivity and hardness measurements during isothermal aging treatments were also conducted. The effects of prior aging and alumina particle additions on the growth kinetics and the thermal stability of the metastable phases in each material were studied. The results were used to characterize the effect of reinforcement on the aging kinetics of composite materials.

Accession For	
NTIS GRA&I	<input checked="" type="checkbox"/>
DTIC TAB	<input type="checkbox"/>
Unannounced	<input type="checkbox"/>
Justification	
By	
Distribution/	
Availability Codes	
Dist	Avail and/or Special
A-1	

iii

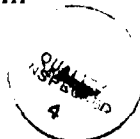


TABLE OF CONTENTS

I. INTRODUCTION	1
A. METAL MATRIX COMPOSITES	1
B. ACCELERATED AGING AND MICROSTRUCTURAL EVOLUTION	3
1. Microstructural Evolution in 6061 Aluminum	3
2. Accelerated Aging	10
C. RESEARCH OBJECTIVE	16
II. DESCRIPTION OF MATERIALS	19
III. EXPERIMENTAL PROCEDURE	20
A. HARDNESS TESTING	20
B. DIFFERENTIAL SCANNING CALORIMETRY	21
C. RESISTIVITY	25
D. TRANSMISSION ELECTRON MICROSCOPY (TEM)	26
IV. RESULTS AND DISCUSSION	28
A. HARDNESS TESTING	28
B. DIFFERENTIAL SCANNING CALORIMETRY	30

1.	Characterization of the DSC Thermogram of Commercial Aluminum Alloy 6061	30
2.	Effect of Al ₂ O ₃ Particles Additions on the Matrix Aging Behavior	37
3.	Effect of Pre-aging on the Precipitation of the Metastable Phases	40
C.	RESISTIVITY	46
V.	CONCLUSIONS	52
	LIST OF REFERENCES	54
	INITIAL DISTRIBUTION LIST	57

I. INTRODUCTION

A. METAL MATRIX COMPOSITES

Metal Matrix Composites (MMCs) are a class of materials which can be designed to combine the ductility, strength and formability of metallic (e.g. aluminum) alloys with the specific modulus (the ratio of the elastic modulus to density) of nonmetallic compounds such as silicon carbide, aluminum oxide, boron carbide, etc. [Ref. 1]. The basic idea is to add the nonmetallic reinforcements to the metallic alloy to form a two phase mixture. The reinforcements can be discontinuous, in the shape of irregular particles or whiskers or they can be continuous filaments or fibers. Regardless of the type of reinforcement, MMCs offer unique opportunities to provide combinations of physical and mechanical properties not achievable in monolithic alloys. Some of these properties include:

- strength (both tensile and shear)
- stiffness
- coefficient of thermal expansion (CTE)
- wear resistance
- weight
- corrosion resistance
- thermal conductivity

Of these properties, the higher stiffness of the MMCs is particularly important since, unlike strength, stiffness is not improved by alloying or heat treating. Also, the lighter weight and the ability to tailor properties such as CTE and thermal conductivity make MMCs especially well suited for use in such applications as electronic packaging and high reliability avionic components.

While MMCs have been available for many years, the field has seen a marked increase in both research and production since Toyota conducted the first commercial trials of selectively reinforced ceramic/aluminum-alloy pistons for diesel engines in the early 1980's [Ref. 2]. Previously, emphasis in this field had been focussed on metal matrices reinforced with continuous fibers of such materials as boron, graphite and silicon carbide. The high cost and difficulty in manufacturing components from these MMCs meant that their use was restricted to aerospace and other high-tech applications. With the development of MMCs that use reinforcements of discontinuous fibers, whiskers, and/or particles, different, lower cost manufacturing techniques could be applied.

The powder metallurgy (PM) technique has been the traditional method of manufacturing MMC materials and components. This technique involves the blending of prealloyed powders of the base metal and the reinforcement and then compacting the mixture using hot isostatic pressing. Additional processing of the composite material is usually required to ensure a uniform distribution of properties. Therefore, the size and complexity of parts that can be manufactured using the PM technique are limited [Ref. 3].

Recently, ingot metallurgy techniques, i.e., casting, have been developed, which show promise as a low cost, high quality alternative to PM techniques. Currently, the only commercial source of castable MMCs is Duralcan USA, San Diego. In its patented manufacturing process, fine ceramic particles are mixed into molten aluminum by vigorous stirring. The particles are thoroughly wetted by the aluminum, and distribution in the cast products is quite uniform [Ref. 4]. Because the manufacturing costs of cast MMCs are low and because they can be shape-cast, the use of these materials has expanded to such industries as sporting goods, automotive, and electro-mechanical machinery. Examples of such expanded use include: a Duralcan extruded tubing tennis racket which provides 25% reduced vibration and increased stiffness, at a lower cost compared with graphite/epoxy rackets [Ref. 1]; and, an aluminum matrix composite containing silicon carbide whiskers which had been forged into turbine wheels in such a way that the whisker reinforcements were radially aligned [Ref. 5].

B. ACCELERATED AGING AND MICROSTRUCTURAL EVOLUTION

1. Microstructural Evolution in 6061 Aluminum

Aluminum 6061 is an age hardenable alloy which contains the following nominal composition of alloying elements [Ref. 6]:

Table I: Composition of 6061 Al								
Si	Fe	Cu	Mn	Mg	Cr	Zn	Ti	Others
0.4 to 0.8	0.7 max	0.15 to 0.40	0.15 max	0.8 to 1.2	0.15 to 0.35	0.25 max	0.15 max	0.15 max total

Although the age hardening behavior of various Al-Mg-Si alloys, including 6061, has been the subject of numerous investigations, there is still some controversy surrounding both the sequence and the composition of the phases.

In his study of high purity, single crystal aluminum alloys, Lutts [Ref. 7] found that the early GP zones (which he called "primitive zones") were needle-shaped with the needle axis oriented along the matrix cube directions. These zones had a high vacancy concentration and no internal order. The second phase of "pre-precipitation" (i.e., precipitation prior to the equilibrium precipitate) was characterized by the establishment of linear periodicity along the segregate axis parallel to one of the matrix cube directions. This periodicity was identical to that of the matrix. Once the equilibrium phase precipitated, the hardness of the alloy decreased. This led to the conclusion that the needle-shaped GP zones were the only hardening agents in these alloys.

Using transmission electron microscopy (TEM) on a high purity Al-Mg-Si alloy, Thomas [Ref. 8] also found that the first stage of precipitation from a supersaturated solid solution was the formation of needles having a $\langle 100 \rangle_{Al}$ growth direction. These zones only existed at temperatures below 220°C. He

concluded that these zones consisted of rows of atoms lying along $\langle 100 \rangle_{Al}$, in such a way that there was one row of silicon atoms between two rows of magnesium atoms. Assuming metallic bonding between the atoms in the zone, he determined that there would be approximately 2% lattice expansion to accommodate the zone, not enough for large scale coherency strains. Since there was no contrast effects around the precipitates, he concluded that the zones were coherent with the matrix with only small elastic coherency strains. At temperatures above 220°C, Thomas found that the needles turned into rods by increasing both in length and in diameter. The density of rods in the matrix, however, decreased. The diffraction patterns corresponding to the rods were consistent with a f.c.c. lattice with a lattice parameter of approximately 6.42 Å. Since the lattice parameter of equilibrium Mg_2Si is 6.39 Å, he concluded that the rods were an intermediate Mg_2Si phase. The final stage of precipitation consisted of platelets of the equilibrium phase Mg_2Si . In most cases, the platelets grew out of the intermediate rod structure, although in some cases, they appeared to nucleate independently. Based on the fact that the equilibrium Mg_2Si tended to leach out of the sample foil during preparation, Thomas concluded that this phase was completely incoherent with the matrix. Finally, Thomas found that, during all stages of aging, precipitation occurred uniformly throughout the matrix; no precipitation was ever observed on dislocations.

Cordier and Gruhl [Ref. 9] studied the precipitation of Al- Mg_2Si alloys during high temperature aging. They found that aging in the range between 160°C and 200°C produced GP zones that were approximately spherical in shape and

whose size depended on the aging time and temperature. In the region of peak hardness, they observed additional small needle-like particles whose size increased with over-aging, while the GP zones disappeared. On prolonged aging the precipitates became plate-like in appearance.

Ceresara *et al.* [Ref. 10] found that, in an Al-Mg₂Si alloy, when the amount of silicon in the alloy exceeded the amount required to form Mg₂Si, the excess Si did not change the nature of the aging process. It did, however, affect both the kinetics (i.e., it increased the rate of the process) and the thermodynamic factors (i.e., it increased the density but decreased the size of the zone). They proposed that the excess Si reduces the solubility of Mg₂Si in an Al compound. Therefore alloys with a constant Mg₂Si content, after quenching from the solution temperature, should be more supersaturated, the higher the Si excess.

Ozawa and Kimura [Ref. 11] set out to determine the operating mechanism to explain the marked enhancement of precipitation in Al-Si alloys that is obtained by conducting a pre-aging treatment of the alloy near room temperature. The two proposed mechanisms were:

- Solute-Cluster Mechanism. Based on this mechanism, Si atoms would be expected to form clusters homogeneously in the matrix during the pre-aging treatment. Quenched-in vacancies would be used to increase the Si atom migration during this stage. Clusters that had reached a critical size during pre-aging would then continue to grow during subsequent, higher temperature aging.
- Vacancy-Cluster Mechanism. Based on this mechanism, excess vacancies would be expected to form clusters (dislocation loops and voids) during the pre-aging treatment. These clusters would then be used as preferential

nucleation sites for the Si precipitates during the subsequent, higher temperature aging. Although this is a heterogeneous nucleation process, the precipitates will be finely distributed within the grains.

The results of their study indicated that the vacancy-cluster mechanism was the applicable one. In addition, they found that pre-aging the alloy at temperatures below a critical temperature of approximately 70°C led to finely distributed precipitates during subsequent aging, while pre-aging above this temperature always yielded a coarse precipitate. This was attributed to the annealing out of vacancy loops at the higher pre-aging temperatures. Finally, their discussion indicated that the migration of Si atoms at room temperature would be too slow (even if it was assisted by an excess vacancy concentration) to be the dominate mechanism for enhancing the precipitation.

Kovacs *et al.* [Ref. 12] found that in Al-Mg₂Si alloys, the clustering process of the solute atoms always began with the precipitation of Si, enhanced by the quenched-in vacancies. In this stage the behavior of the alloy was very similar to the behavior of the Al-Si alloy system. In the following phase, Mg and Si atoms from the solution precipitate on the Si nuclei. The precipitation of Mg is probably enhanced by the strong Mg-Si interaction within the zone. In the final stage, the concentration of Mg within the zone becomes high enough for the formation of Mg₂Si nuclei. This is evidenced by a decrease in the resistivity of the alloy. At this stage, further growth of Mg₂Si precipitates takes place by simple diffusion. Kovacs *et al.* also presented a hypothesis to explain the effect of pre-aging on the

precipitate size and distribution during subsequent higher temperature aging. For pre-aging below the critical temperature (T_{cr} , approximately 70°C), zone formation occurs on finely distributed Si precipitates. If the duration of pre-aging is short, most of the alloying elements remain in solid solution. During the subsequent higher temperature aging (above T_{cr}), almost no new nucleation takes place; further precipitation takes place on the nuclei formed during pre-aging. With increasing pre-aging time, the number of zones increases, thus decreasing the concentration of alloying elements within the solid solution. As a result, a longer time is required at the higher aging temperature in order to obtain the critical size particle and/or the critical Mg concentration within the zone. This is because the concentration of alloying elements within the solid solution is insufficient to support the process. Thus some of the zones will have to dissolve, a process that is very slow due to the strong binding between the Mg and Si atoms. With increasing pre-aging time, the stability of the zones increases, thus increasing the time required to dissolve them.

Smith [Ref. 13] studied the effect of reversion treatments on an Al-Mg₂Si alloy. He found that two types of precipitates, one of which was approximately spherical while the other was needle-like, were present in the material in the peak hardness condition. He concluded that GP zones were not the only hardening agents in these alloys, as proposed by Lutts [Ref. 7], but that they were, in fact, strengthened by both GP zones and the intermediate partially coherent phase. His results also agreed more with Cordier and Gruhl's work [Ref. 9] in that the GP

zones appeared to be spherical-like and the intermediate β' precipitate appeared to be needle-like.

Lendvai *et al.* [Ref. 14] also found that when Al-Mg-Si alloys were quenched to temperatures above T_{cr} , that the change in resistivity was severely reduced (for short duration aging above T_{cr}) or essentially zero (for slightly longer times above T_{cr}). Their explanation for this was based on the mechanism of vacancy enhanced nucleation of Si proposed by Ozawa and Kimura [Ref. 11]. According to this mechanism, the formation of dislocation loops by vacancy condensation can only occur at temperatures for which $\Delta E < kT \ln(n_q/n_o)$, where ΔE is the energy increment caused by a vacancy absorption into a dislocation loop and n_q and n_o are the number of quenched-in and equilibrium vacancies respectively. When the reverse inequality is applied, it means that there is virtually no vacancy condensation into dislocation loops above T_{cr} . Therefore, Si clustering must occur at other heterogeneities which exist in much smaller numbers within the material. This explains the virtually zero change in resistivity for all but very short times above T_{cr} . If the aging time above T_{cr} is very short, the excess vacancy concentration is not completely reduced. Then if further aging is carried out below T_{cr} , the zone formation process will still start by the vacancy enhanced mechanism but the total number of dislocation loops will be reduced leading to a reduction in the resistivity change.

Finally, while most authors agree that the general sequence of age hardening for Al-Mg-Si alloys is: GP zones \rightarrow intermediate phases \rightarrow equilibrium

Mg₂Si, the exact details are still unclear. The most elaborate sequence that has been proposed so far is [Ref. 15]: supersaturated solid solution → vacancy-silicon clusters → vacancy rich coherent Al-Mg-Si GP zones → disordered, partially coherent $\langle 100 \rangle_{\text{Al}}$ needle-shaped phase → ordered, partially coherent $\langle 100 \rangle_{\text{Al}}$ needle-shaped phase → semicoherent, hexagonal (a = 7.05 Å, c = 4.05 Å) rod-shaped phase → semicoherent, hexagonal (a = 7.05 Å, c = 12.15 Å) rod-shaped phase → equilibrium Mg₂Si platelets. Another area of controversy is the morphology of the GP zones.

While many authors propose that GP zones have a needle-like shape, some authors [Refs. 9 and 13] believe the zones are more nearly spherical.

2. Accelerated Aging

The reinforcements used to make MMCs are typically high melting point, relatively inert materials. For example, while the melting range of 6061 Aluminum is 582°C - 649°C, the melting point of Al₂O₃ is 2037°C [Ref. 6]. As such, the reinforcements would not be expected to significantly alter the chemistry of the matrix alloy or to radically effect the age-hardening characteristics of the material. This, however, has not been the case. Studies of many precipitation hardened MMCs have found that the aging characteristics of the composite have been accelerated relative to the characteristics of the unreinforced, monolithic alloy. Nieh and Karlak [Ref. 16] found that B₄C particles significantly accelerated the aging of the 6061 aluminum matrix relative to that of the monolithic 6061 control material. They found that the addition of a high volume percent (23 vol%) of B₄C to 6061-Al accelerated its aging response, especially at low temperatures. The matrix of the

composite reached its peak hardness in approximately 3 hours at 177°C, while the unreinforced material took approximately 10 hours. They attributed this to the high dislocation density which was generated by the thermal contraction mismatch (5:1) between the reinforcement and the matrix, and to the presence of a high diffusive interface in the composite.

A similar result was obtained by Dutta *et al.* [Ref. 17] who studied the aging response of a 6061Al - 10 vol% SiC whisker MMC. They found that at an aging temperature of 205°C, there was a reduction in the peak aging time from 100 minutes for the monolith to 50 minutes for the MMC.

Christman and Suresh [Ref. 18] studied a SiC whisker reinforced 2124-aluminum matrix composite and found that the addition of 13.2% SiC whiskers led to a reduction of the peak aging time from 12 hours for the monolith to 4 hours for the composite at the aging temperature of 177°C. Their findings also showed that the peak and unaged microhardness of the composite was essentially the same as that of the monolith.

There are two primary theories to explain the mechanism of accelerated aging in MMCs [Refs. 16, 18 and 19]. The first theory is that the high dislocation density in the vicinity of the reinforcements enhances the nucleation of precipitates. The second theory is that residual stress fields caused by the differential thermal contractions of the matrix and the reinforcement act as short-circuit paths for diffusion of the solute atoms.

Based on the results of their study, Christman and Suresh [Ref. 18] proposed that the significantly accelerated aging phenomenon in the MMC was due to the high dislocation density that was developed because of the large thermal contraction mismatch between the aluminum matrix and the SiC (10:1). The dislocations in the matrix of the composite served as nucleation sites for the strengthening precipitates during the aging of the composite and thus facilitated the attainment of peak matrix hardness at much shorter times than in the control alloy.

The evidence they used to support this theory included:

- TEM studies of the Al-SiC composite material which revealed the significantly higher dislocation density over that of the unreinforced material.
- During the initial stages of precipitation, the nucleation of strengthening precipitates preferentially occurred on the dislocations.
- The results of *in situ* TEM studies conducted by Vogelsang *et al.* [Ref. 20] which demonstrated the punching of dislocations at whisker ends *during* cooling from the annealing temperature in a Al-SiC composite.
- The fact that their (Christman's and Suresh's) TEM observations did not indicate any preferential precipitation at or near the interfaces in 2124-SiC composite. They noted that preferential precipitation would have been expected if the residual stresses, which were not relieved by the punching of dislocations during cooling, were responsible for accelerated aging. Furthermore, they could not detect any precipitate-free zones near the interface region.
- The results of their parallel studies on the effect of cold working (which leads to higher dislocation densities) on the aging behavior of the unreinforced material. These studies showed an accelerated aging behavior in the cold worked material which was similar to that of adding SiC reinforcements.
- The results of calculations of dislocation punching distances at whisker ends which provided theoretical justification for the possibility of an almost

complete coverage of the matrix of the Al-SiC composite with an enhanced dislocation density.

In his study of various aluminum matrix composites prepared by both powder metallurgy and casting processes, Papazian [Ref. 21] found that it was only the precipitation of certain intermediate phases that was accelerated by the addition of SiC. He attributed this to the higher dislocation density in the composite. He found that the kinetics of the GP zone formation and dissolution and the intermediate phase formation were accelerated relative to the wrought alloy primarily due to the powder metallurgy process and to a lesser extent due to the SiC reinforcement.

Suresh *et al.* [Ref. 22] found accelerated aging occurred in aluminum matrix composites containing 6%, 13%, and 20% by volume SiC particulates. The peak-aging time for the unreinforced alloy was about 60 hours at the aging temperature of 190°C. However, all the composite materials reached peak hardness in the matrix within a time span of 16 to 24 hours at the same aging temperature. As in their previous work [Ref. 18], they attributed this acceleration to the higher dislocation density in the composite materials. Their results indicated that even a 6 vol% of SiC particles in the aluminum matrix generated enough dislocations for the heterogeneous nucleation of the strengthening precipitates. Further increases in SiC volume fractions did not lead to any noticeable enhancements in the matrix dislocation density. Consistent with this trend, the peak-aging times for the three composite materials did not exhibit any significant differences. They also noted that

the dislocation densities measured in the particulate reinforced materials were a factor of three smaller than those obtained previously in the whisker reinforced material. Another interesting feature noted by Suresh *et al.* [Ref. 22] is that the unreinforced alloy and the matrices of all the composite materials exhibited essentially the same microhardness in the solutionized and as-quenched condition. Since there is a linear relationship between hardness and strength, this result implies that the enhanced dislocation densities in the matrices of the composite do not markedly contribute to the strengthening of the material despite their profound effect on aging. This observation is at variance with the suggestions of other researchers [Ref. 20 and 23] that the high dislocation density is the major reason for the high strength of MMCs.

The second theory for accelerated aging is the enhancement of the diffusion of solute atoms due to the generation of an elastic residual stress field in the matrix around the reinforcement as a result of quenching. The solute atoms will use this macroscopic residual stress field in the same way that they use the microscopic stress fields around dislocations, i.e., as a short-circuit path for diffusion. The basis of this stress-assisted diffusion is that the larger solute atoms will migrate toward the tensile stress field and the smaller solute atoms will migrate toward the compressive stress field, thereby lowering the total strain energy of the system. Since the solute atoms will migrate preferentially to certain areas of the matrix, the nucleation and/or growth of the precipitates will be enhanced.

Dutta and Bourell [Ref. 19] developed a theoretical model and experimentally studied an aluminum alloy 6061 reinforced with 10 vol% SiC whiskers of variable aspect ratios to identify which of the two mechanisms controls the rate of accelerated aging. They found that the dominant operative mechanisms of accelerated aging of MMCs depend on several factors, including the size and the volume fraction of the reinforcement for a given composite system. In composites with very high dislocation densities (10^{14} m^{-2} or higher) and large fiber radii ($1 \mu\text{m}$ or greater), the dislocation mechanism should dominate. In composites with dislocation densities lower than 10^{13} m^{-2} and reinforcement radii smaller than $0.25 \mu\text{m}$, the residual stress mechanism is expected to dominate. A theoretical model was developed which predicted that there was a range of reinforcement radius values over which both mechanisms gave comparable precipitation rates. The upper and lower limits of this range depend on the reinforcement morphology, on the distribution and volume fraction of the reinforcement, on the temperature range of quenching and on the matrix dislocation density for a given composite system. While the usual range of reinforcement diameters of commercially available SiC-whisker-reinforced 6061 aluminum ($0.3 \mu\text{m}$ to about $3 \mu\text{m}$) and the usual value of dislocation densities ($5 \times 10^{13} \text{ m}^{-2}$) indicate that, theoretically, both mechanisms should be operating, the experimental results indicate that the accelerated aging is dominated by dislocation-enhanced nucleation and/or growth rather than residual-stress-induced diffusion. They hypothesized that locally the stress field of a dislocation overwhelms the long-range hydrostatic residual stress field of the fiber,

thereby resulting in solute atom entrapment on dislocations rather than diffusion down the stress gradient.

C. RESEARCH OBJECTIVE

Although a good deal of work has been done recently to characterize the aging behavior of precipitation hardenable metal matrix composites there are several areas where additional research is needed.

Most of the previously published studies have been done on composite materials that were prepared using the powder metallurgy process. As reported by Papazian [Ref. 21], this process produces accelerated aging effects of its own and therefore masks the aging effects due to nonmetallic reinforcements. Only one of the composites in Papazian's study was not manufactured by the powder metallurgy process. This material was a cast aluminum alloy 7475 reinforced with SiC particulates. The other study that used a cast material was the work done by Suresh *et al.* [Ref. 22]. Their material was a high purity Al-3.5 wt% Cu alloy reinforced with SiC particulates. In both studies, the cast composites exhibited accelerated aging relative to the monolithic matrix material.

Almost all of the published studies have used aluminum matrix materials reinforced with SiC. Since the ratio of the coefficients of thermal expansion (CTEs) of the aluminum versus the SiC is about 10:1 (i.e., $\alpha_{\text{SiC}} \sim 3 \times 10^{-6} / \text{K}$ and $\alpha_{\text{Al}} \sim 23 \times 10^{-6} / \text{K}$), a very high dislocation density due to differential thermal contraction on cooling is expected. Only the study done by Nieh and Karlak [Ref. 16] used a

different reinforcement - 23 vol% B₄C. Here, although the ratio of CTEs is much smaller (approximately 5:1), the significantly higher volume percent of reinforcement was expected to have an effect on the matrix microstructure. The CTE of Al₂O₃ is about $7 \times 10^{-6} / \text{K}$, making the CTE ratio of Al to Al₂O₃ about 3:1. Therefore, alumina reinforced aluminum matrix composites would be expected to exhibit little, if any, accelerated aging, especially if the reinforcement volume fraction is low.

Many of the published studies used reinforcements in the form of whiskers vice particles. Suresh *et al.* [Ref. 22] found that the dislocation densities generated by particles is a factor of three lower than the densities generated by whiskers, reducing the tendency to accelerate aging.

On the basis of these discussions, it is clear that a detailed study of the aging kinetics in cast alumina reinforced aluminum matrix composites is necessary. The only known work that used this material is the research conducted by Hafley [Ref. 24], who studied the effect of 15 vol% alumina particle reinforcements on the aging behavior of cast 6061 aluminum matrix composite. The purpose of the present work is to study the effect of additions of 10 vol% and 15 vol% alumina particles on the aging characteristics of the cast 6061 aluminum matrix composite. The main areas of interest are: (1) Determining if the stresses caused by the smaller differential CTEs and the smaller volume percents of alumina (i.e., 10 - 15 vol% Al₂O₃ versus 23 vol% B₄C) are sufficient to effect the aging behavior of this

material. (2) Assuming that the Al_2O_3 does effect the aging characteristics of the material, determining the effect on the early stages of precipitation.

II. DESCRIPTION OF MATERIALS

The composite materials used in this study were fabricated by Dural Aluminum Composites Corporation, San Diego, California, using a proprietary casting technique. The matrix material was commercial 6061 aluminum, which was reinforced with 10 volume percent and 15 volume percent alumina particles. The alumina particulate had irregular shapes and ranged in size from about 0.5 μm to 25 μm . The composite was hot-extruded after casting to homogenize the microstructure and was supplied as a bar with a 7.6 cm x 1.9 cm cross section.

The control material, a monolithic commercial 6061 aluminum alloy, was obtained from ALCOA. This material was produced by ingot metallurgy techniques and was supplied as hot-rolled stock.

III. EXPERIMENTAL PROCEDURE

A. HARDNESS TESTING

The microhardness measurements of the Al-10 vol.% Al₂O₃ composite, aged at 200°C were obtained using the Buehler Micromet Vickers Microhardness Tester with a 100 gram load. Nine samples, measuring approximately 1.9 cm x 1.2 cm x 0.4, were cut using a band saw and then machined to final size using diamond tipped tooling. One side of all samples was sanded, using a series of sandpapers ranging from 240 grit to 600 grit. This was done in order to provide a smooth surface for the indenter. The samples were then wrapped in aluminum foil to minimize surface oxidation during the solutionizing treatment. All samples were solutionized in a horizontal tube furnace, at approximately 545°C for 90 minutes and quenched in ice water. After quenching, the samples were removed from the aluminum foil, dried, rewrapped in aluminum foil (both to minimize surface oxidation during aging and to facilitate handling), and placed in the 200°C aging furnace. The aged samples were then removed from the furnace at various times and quenched in ice water to stop the aging process. After quenching, the samples were removed from the aluminum foil, dried and stored in a freezer at 0°C until the hardness measurements could be taken. When doing the hardness measurements, an average of five readings were taken from each aged sample. Care was taken to ensure that the indenter was hitting only the matrix material but that it was close enough to the

reinforcing particles so that its effects could be felt. The results of the hardness measurements were then converted to a Vickers Hardness Number.

B. DIFFERENTIAL SCANNING CALORIMETRY

The changes in heat flow as a function of temperature, for both composite materials and the monolithic alloy, were measured using the Perkin-Elmer Model 2C Differential Scanning Calorimeter (DSC). A strip, measuring approximately 1.5 mm thick, was cut from each of the three materials using a band saw. DSC sample disks, measuring 5.5 mm in diameter, were then cut from each material using electric discharge machining. The samples were sanded until they were all approximately the same size and weighed using an analytical balance. A DSC reference of essentially pure aluminum was prepared using a number of DSC sample pan lids, so that the mass of the reference was approximately the same as the mass of the composite and monolithic samples. Each sample was solutionized in the horizontal tube furnace using an argon purge to minimize oxidation. The solutionizing treatment was conducted at approximately 545°C, for 90 minutes. The samples were then quenched in ice water, dried and placed directly into the DSC. The time at room temperature, prior to placement in the DSC, was less than ten minutes. Five different aging treatments were conducted for the monolithic alloy and 10 vol% Al₂O₃ composite:

1. No aging
2. Aged at 298K for 90 minutes in the DSC

3. Aged at 313K for 90 minutes in the DSC
4. Aged at 323K for 90 minutes in the DSC
5. Overaged at 473K for 72 hours

Only treatments 1 and 5 were used for the 15 vol% composite.

The following parameters were set for all runs:

- Lower Temperature Limit - 270K
- 273K (for the computer)
- Upper Temperature Limit - 833K (for treatment 1)
- 633K (for treatments 2, 3, and 4)
- Heating Rate - 10K/minute
- Energy Setting - 5 mcal/s
- Sample Chamber Purge Gas - Nitrogen 95% pure (Note - An additional drying tower was added prior to the DSC to minimize moisture.)
- Glove Box Purge Gas - Nitrogen 95% pure (Note - A drying tower was also added here.)
- Chart Recorder Settings - Pen 1 - 10 mv full scale
- Pen 2 - As low as possible for initial exothermic peak

The heat flow versus temperature data for each run was subsequently converted to ΔC_p versus temperature by subtracting a baseline representing the aluminum-rich solid solution with existing precipitates. This baseline was obtained by scanning the overaged sample from 273K to 800K and extrapolating the plot to 833K.

The first exothermic peak, which was only observed in the monolithic alloy and the Al-10 vol% Al₂O₃ composite and which was tentatively assigned to the formation of Si-clusters, was replotted on an enlarged scale for each experiment. The total and partial areas under the curve were obtained by carefully cutting out and sectioning the curve and then weighing the pieces on the analytical balance. A rectangular section of the graph was also cut out and weighed and was used for scale conversion. The results of this method were checked using the planimeter. Once the areas were obtained, the specific reaction rate constant (k_r) was calculated for several temperatures within the curve, using the following formula:

$$k_r = \frac{Q\Delta C_p}{A - a_t}$$

where:

Q is the constant heating rate (in this case, 10K/min)

ΔC_p is the change in heat capacity at the selected temperature (J/K-mole)

A is the total area under the curve (J/mole)

a_t is the partial area under the curve up to the same temperature (J/mole)

Then, absolute reaction rate theory [Ref. 25] was applied and the activation energy, E_a , the activation entropy, ΔS , the activation enthalpy, ΔH , and the free energy of activation, ΔG were obtained by using the following formulae [Ref. 26]:

$$E_a = \frac{RT^2 d(\ln K_r)}{dT}$$

$$\Delta H = E_a - RT$$

$$\Delta S = \frac{\Delta H}{T} + R \ln\left(\frac{hk_r}{kT}\right)$$

$$\Delta G = -RT \ln\left(\frac{hk_r}{kT}\right)$$

where:

R is the universal gas constant (8.314 J/K-mole)

T is the temperature of interest (K)

$d(\ln k_r)/dT$ is the slope of the $\ln k_r$ versus temperature curve

at the temperature of interest

h is Planck's constant (6.626×10^{-34} J/s)

k is Boltzmann's constant (1.381×10^{-23} J/K)

C. RESISTIVITY

The changes in resistivity during isothermal aging of the Al-10 vol% Al₂O₃ were measured using essentially the same setup as Hafley [Ref. 24]. Minor changes were made to the rig prior to this set of experiments. These changes included: adding stainless steel weights to all four electrodes to improve contact with the sample (Note - the center two electrodes were cut down to prevent contact between electrodes); manufacturing new stainless steel guide rails and supports for the top plate to reduce the play in the top plate; and manufacturing a new machinable ceramic support for the sample to ensure that the sample was centered beneath the electrodes. Once the rig was modified, thin strips of the composite were cut using a band saw and machined with diamond tip tooling to a final size of 115 mm x 3.87 mm x 1.77 mm.

Each sample was solutionized in the horizontal tube furnace at approximately 545°C for 90 minutes and quenched in ice water. During the solutionizing treatment, the samples were wrapped in aluminum foil, both to protect the sample from damage (e.g. nicks, scratches, etc.) and to minimize surface oxidation. This step was not really necessary, since Osamura and Ogura [Ref. 27] found no significant differences between the electrical resistivity curves for specimens solutionized in a purified argon atmosphere and for specimens solutionized in air.

They suggested that the surface oxidation did not affect the essential features of the precipitation process.

After quenching, the aluminum foil was removed, the samples were dried and they were immediately placed in the furnace. The resistivity changes were measured during isothermal aging at the following temperatures: 20°C, 51°C, 100°C and 200°C. Data on the resistivity changes was collected for 30 hours for all aging treatments except 20°C. For these samples, data was collected for 72 hours. In all cases, the computer program RESIST.BAS [Ref. 24] was set to acquire data every 5 seconds for the first 5 minutes, every 30 seconds for the remainder of the first hour and every 5 minutes thereafter.

D. TRANSMISSION ELECTRON MICROSCOPY (TEM)

TEM samples of both the monolithic 6061 alloy and the Al-15 vol% Al₂O₃ were prepared by slicing an approximately 0.25 mm thick foil of each material using a low speed diamond saw. Disks 3 mm in diameter were then punched from the foil. The disks were thinned to a final thickness of 100 - 150 microns using 600 grit sandpaper. After thinning the samples were cleaned in acetone and air dried. The samples were placed in aluminum DSC pans, covered and then wrapped in aluminum foil. The samples were solutionized in the horizontal tube furnace at approximately 545°C for 90 minutes and then quenched in ice water. The monolithic 6061 samples were given the appropriate heat treatments in the DSC to study the microstructures present in the alloy after each DSC exothermic peak.

For all heat treatments, the heat rate was 10K/min and the autocool rate was 320K/min. A monolithic 6061 TEM sample was also heat treated in a 200°C furnace for 50 seconds and quenched in ice water. The composite TEM samples received the following heat treatments: Solutionized and quenched - no additional heat treatment; and 315 seconds in a 200°C furnace and quenched in ice water. After the heat treatment, the monolithic 6061 TEM samples were electropolished using a Struers Tenupol twin-jet system. The electropolish solution was 3% perchloric acid, 62% ethanol, and 35% butoxy-ethanol. The voltage was 20V, the temperature of the polishing solution was -30°C to -40°C and the Tenupol pump flow rate was 4.5. The composite samples were thinned using an ion mill. Once the samples were thinned, they were stored in a freezer at 0°C until they could be examined under the TEM. A JEOL 100CX transmission electron microscope operating at an accelerating voltage of 120V was used for all observations.

IV. RESULTS AND DISCUSSION

A. HARDNESS TESTING

Figure 1 shows the results of the hardness measurements of the 10 vol% Al_2O_3 composite, as well as the hardness measurements of the monolithic 6061Al and the 15 vol% Al_2O_3 composite which were obtained by Hafley [Ref. 24]. There are several interesting features of this Figure:

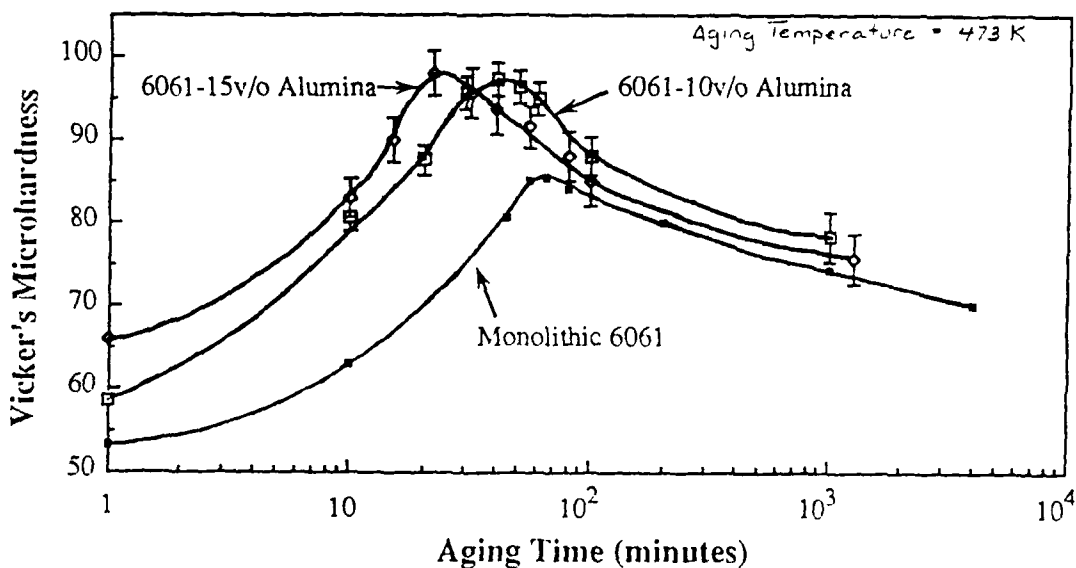


Figure 1: The variation of matrix microhardness as a function of aging time (at 200°C) for the 6061Al alloy with 0, 10 and 10 vol% Al_2O_3 particles.

First, the solutionized and as-quenched matrix microhardness increases with increasing alumina additions. This indicates that the enhanced dislocation densities in the matrices of the composite contribute to the increased strength of these materials. This result is in agreement with several other researchers [Refs. 20 and

23] but is at variance with the results obtained by Suresh *et al.* [Ref. 22]. They found no significant difference in the microhardnesses of the monolith and the composites in the solutionized and as-quenched condition.

Second, the addition of 10 vol% Al_2O_3 particles decreases the time to peak hardness from 70 minutes in the monolith to 40 minutes in the MMC. The addition of 15 vol% Al_2O_3 decreases the time still further, to approximately 200 minutes. Although the addition of 5 vol% more alumina (i.e. 15 vol% vice 10 vol%) further accelerates the time to peak microhardness, the actual value of the peak hardness for the two composites is essentially the same.

Third, the microhardness of the matrices of the composites start out higher than the microhardness of the monolith and remain higher up to the peak hardness. Beyond this point, however, there is no significant difference between the hardness of the overaged monolith and the hardness of the overaged composites. This would indicate that in the early stages of aging, both the matrix dislocation density and the precipitation of the metastable phases contribute to the overall matrix microhardness. As aging progresses toward the peak hardness, however, the influence of the matrix dislocations becomes less pronounced. This would explain why the peak hardness of both composites is essentially the same. Finally, in the overaged condition, the matrix dislocations contribute very little to the microhardness and therefore, the difference between the microhardness of the monolith and the microhardness of the composites is negligible.

Finally, there is a good deal of scatter in the readings taken on the composites, but very little scatter in the monolith readings. This is due to the fact that the microstructure of the monolith is fairly uniform, while the microstructure of the composites is not. Therefore, the value of the microhardness reading depends on the location at which the reading was taken.

B. DIFFERENTIAL SCANNING CALORIMETRY

1. Characterization of the DSC Thermogram of Commercial Aluminum Alloy 6061

Figure 2 shows the thermogram of the solutionized and quenched 6061Al alloy. Four exothermic formation peaks, including one at 355K (A), two partially overlapping peaks close to 515K (B) and 569K (C), and one at 767K (D) are

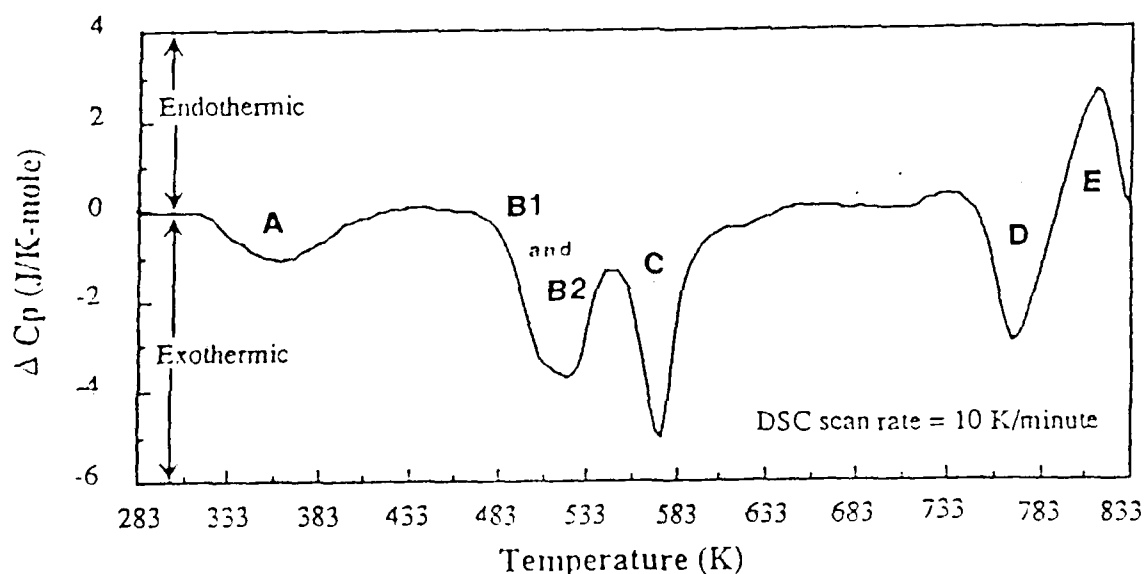


Figure 2: DSC thermogram of solutionized and as-quenched monolithic 6061Al alloy.

apparent, followed by an endothermic dissolution peak at 820K (E). A close observation of Figure 2 suggests that the peak B is actually an unresolved doublet consisting of two superimposed peaks, which will be called peaks B1 and B2.

Figure 3 is the TEM micrograph of a sample heat treated in the DSC up to 400K to reveal the precipitates corresponding to peak A. A high density of very tiny (approximately 10 Å in diameter) precipitates is observed. The corresponding $[001]_{Al}$ selected area diffraction pattern (SADP) does not show any features that are representative of these precipitates. This indicates that the precipitates are fully coherent with the matrix and are only visible due to strain contrast. The faint rings around the transmitted spot are thought to be due to impurities in the sample. As reported earlier [Refs. 8, 10, 12 and 15], the precipitation of Si at vacancy-clusters

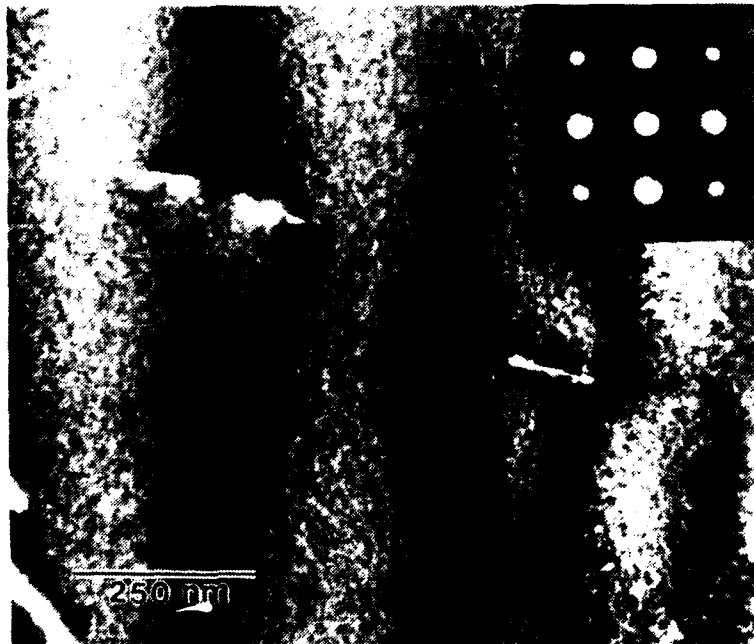


Figure 3: TEM micrograph of the monolithic alloy showing the precipitates corresponding to peak A. The sample was heated in the DSC at 10K/min up to 400K.

is considered to be the first step in the aging of Al-Mg-Si alloys. This suggests that peak A is probably associated with the formation of Si-clusters.

Figure 4 shows the precipitates corresponding to peak B1 in a sample heat treated in the DSC up to 505K. The bright field (BF) micrograph (zone axis= $[001]_{Al}$) reveals the strain contrast due to two kinds of precipitates. Most of the precipitates appear as tiny dots about 50 Å in diameter, while a few are short, thin needles lying along $[010]_{Al}$ and $[100]_{Al}$. Some of the dots might be needles viewed end-on, but if all of them were this configuration then there would have to

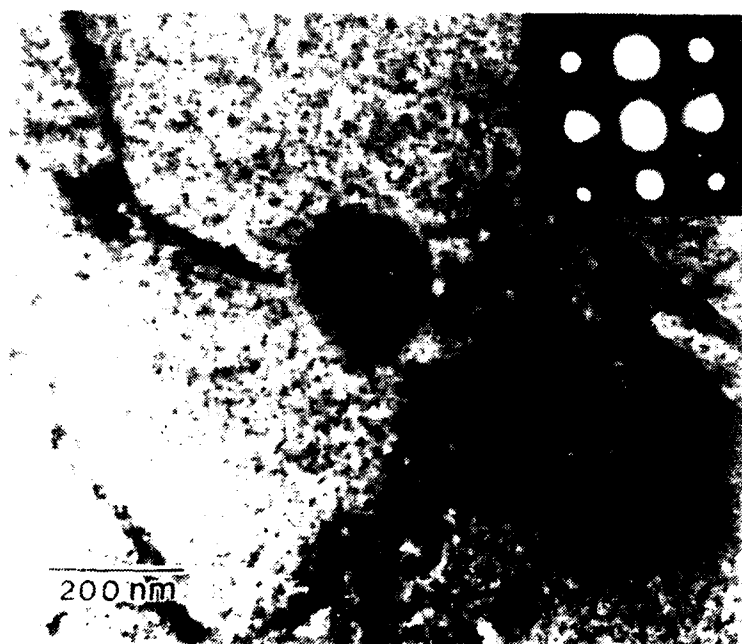


Figure 4: TEM micrograph of the monolithic alloy showing the precipitates corresponding to peak B1. The sample was heated in the DSC at 10K/min up to 505K.

be half as many dots as needles. This is due to the fact that, in foils in the [001] orientation, all three $\langle 001 \rangle$ orientations are equally frequent [Ref. 8]. Since there are obviously much more, not less, dots than needles, the majority of these dots must represent very small precipitates with unresolved shapes. The SADP reveals faint streaks along $\langle 100 \rangle_{Al}$, representative of the few needle-like precipitates [Refs. 8, 15, 28 and 29]. Therefore, the microstructure of a sample heated to the middle of the B1 peak will consist of mostly dot-like and some needle-like precipitates.

Figure 5a shows the BF micrograph and the SADP of a sample heat treated in the DSC up to 515K (i.e. to the middle of peak B2). Here the principle precipitate present is needle-shaped (approximately 100 Å long and 50 Å in

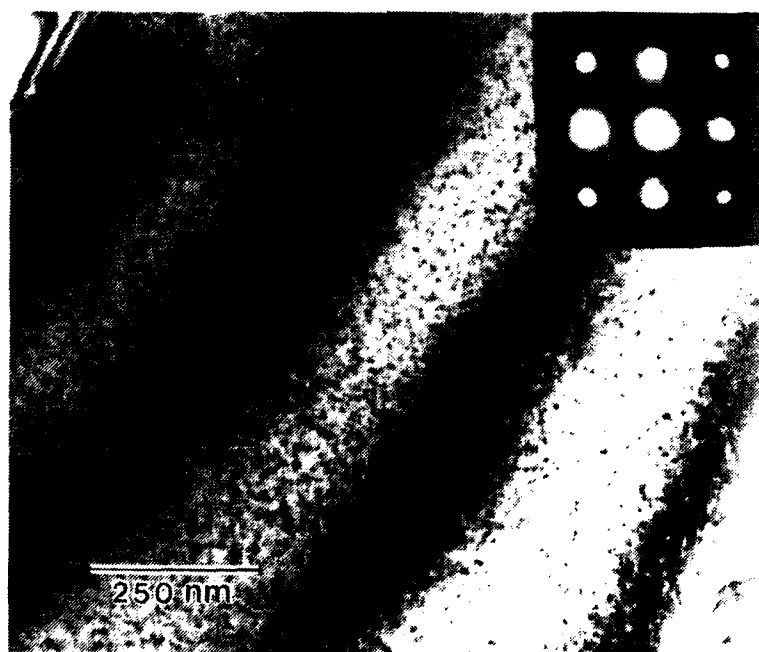


Figure 5a: TEM micrograph (BF and associated SADP) of the monolithic alloy showing the precipitates corresponding to peak B2. The sample was heated in the DSC at 10K/min up to 515K.

diameter). Streaks similar to those in Figure 4 (B1) are visible but are considerably stronger. Since long-exposure SADPs obtained with a defocussed condenser lens failed to produce streaking of the transmitted spot, the streaks are not considered to be a shape-effect. This is supported by an examination of the centered dark field (CDF) image with $g=\bar{2}00$ shown in Figure 5b, where one variant of the needles (those which have their axes parallel to $g=\bar{2}00$) disappears, suggesting that the precipitates are visible primarily due to a matrix strain along $[200]_{Al}$, i.e., perpendicular to the needle axes. In addition to this matrix strain, it is conceivable that there is also a strain in the $\langle 100 \rangle_{Al}$ directions which gives rise to the streaks in the SADP. The intensity modulation along these streaks is probably attributable to the development of a structural periodicity (order) in the needles perpendicular

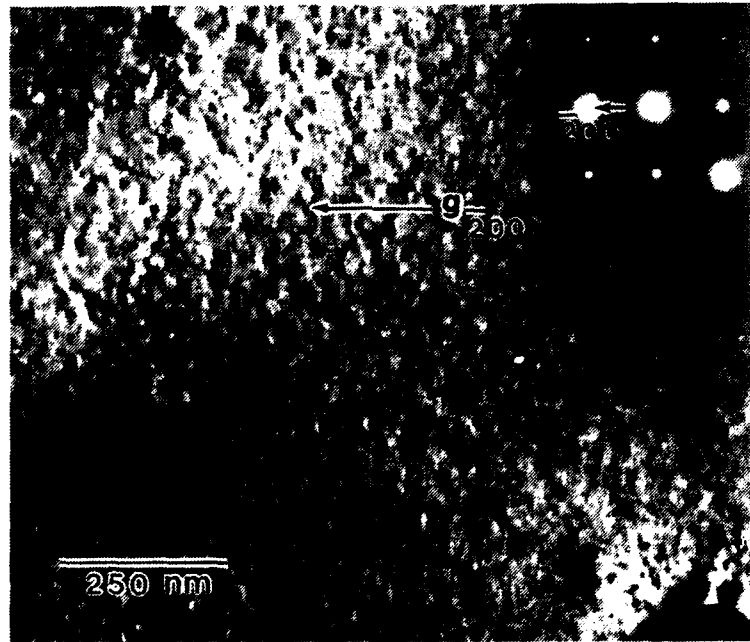


Figure 5b: TEM micrograph (CDF) of the same sample as Figure 5a??? showing the disappearance of one variant of needles.

to their axes [Ref. 28]. Thus the DSC exotherm B2 represents the formation of an ordered needle-shaped phase.

Due to the superposition of the B1 and B2 peaks and to the relatively slow quench rate (320K/min) attained in the DSC, it is entirely possible that the small number of needles observed in Figure 4 (B1) were actually from the start of the B2 peak, while the dots were actually the precipitate formed in the B1 peak. Therefore, it is proposed that the peak B1 represents the formation of very tiny GP-I zones of unresolved shapes, while the peak B2 represents the formation of ordered, needle-shaped GP-II zones (or β''). Although it is generally believed that GP zones in Al-Mg-Si alloys are needle-shaped [Refs. 7, 8, 15, 28 and 29], Cordier and Gruhl [Ref. 9] observed evidence of approximately spherical GP zones, while Smith [Ref. 13] observed a duplex precipitate morphology consisting of both spherical and needle-like GP zones in the peak-aged alloy. Based on the results of this study, it is clear that the near-spherical precipitates observed by other investigators correspond to GP-I zones, while the needle-like precipitates correspond to GP-II zones.

Figure 6 shows the BF micrograph and the corresponding $[001]_{Al}$ SADP of a sample heat treated in the DSC up to 587K (i.e., to the end of peak C). The GP-II or β'' needles in Figure 5a are observed to have grown into rods which are approximately 100-500 Å in diameter and 500 nm in length. Because of the large length-to diameter ratio of the precipitates, a shape effect is now discernible, as evident from the streaking of the transmitted spot along $\langle 100 \rangle_{Al}$. In addition,

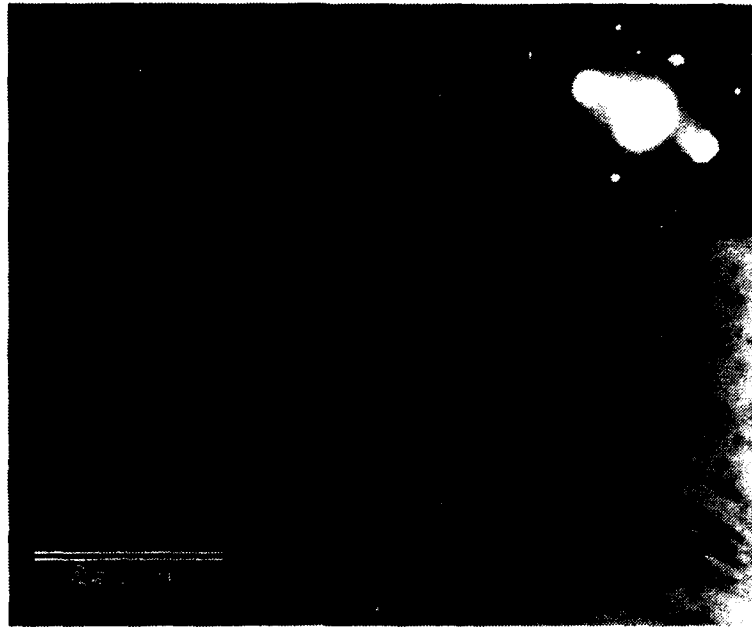


Figure 6: TEM micrograph (BF and associated SADP) of monolithic alloy showing precipitates corresponding to peak C. The sample was heated in the DSC at 10K/min up to 587K.

streaks through both {100} and {200} spots with lengthwise intensity modulations similar to those corresponding to the hexagonal rod-shaped phase identified by Jacobs [Ref. 29] are also visible. These rod-like precipitates correspond to the transition β' -Mg₂Si [Refs. 8, 13 and 15]; therefore, peak C represents β' formation. A sample heated to 760K in the DSC was also examined under the TEM, and as expected [Refs. 17 and 21], incoherent platelets of equilibrium β -Mg₂Si were observed to grow from the β' rods, indicating that the exotherm D represents β formation. The final endothermic peak E represents the dissolution of the β -phase.

In summary, peak A corresponds to Si-cluster formation, peak B is a convoluted peak consisting of GP-I formation and GP-II/ β'' formation, peak C corresponds to β' formation, peak D corresponds to equilibrium β -Mg₂Si formation and peak E corresponds to β -Mg₂Si dissolution. Therefore, the sequence of aging

in commercial 6061 aluminum appears to be: supersaturated solid solution → vacancy clusters/loops → Si-clusters → coherent nearly spherical GP-I zones → semicoherent needle-like GP-II/ β'' → semicoherent rod-shaped β' → incoherent platelets of β - Mg_2Si .

2. Effect of Al_2O_3 Particles Additions on the Matrix Aging Behavior

Figure 7 shows the DSC thermograms of the monolithic 6061 alloy, the

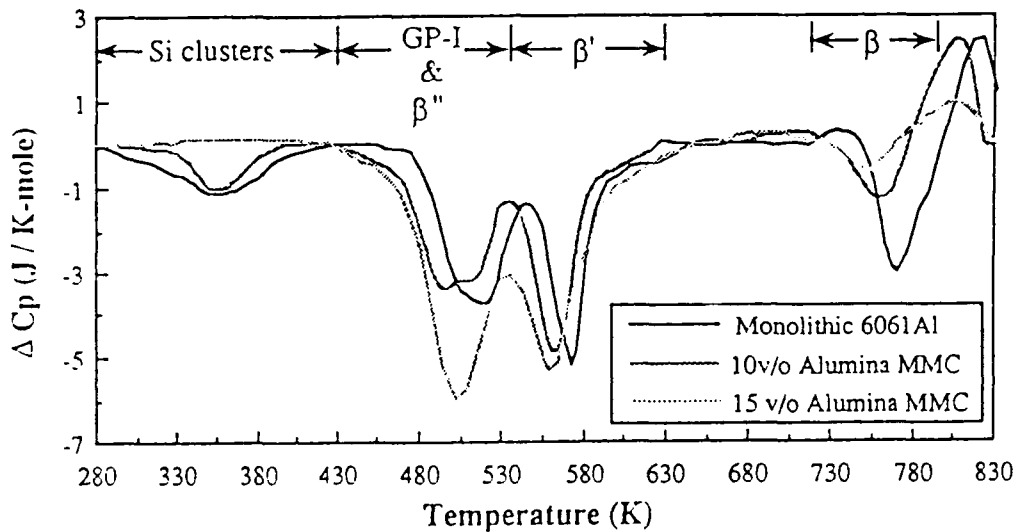


Figure 7: DSC thermograms of solutionized and as-quenched alloys reinforced with 0, 10 and 15 vol% Al_2O_3 particles.

Al 6061-10 vol% Al_2O_3 MMC and the Al 6061-15 vol% Al_2O_3 MMC. All three samples were in the solutionized and as-quenched condition. There are several distinct features that can be observed in this figure:

First, the exothermic peak corresponding to the Si-cluster formation is smaller for the 10 vol% Al_2O_3 than for the monolith and it has totally disappeared for the 15 vol% Al_2O_3 . This result could be interpreted in one of two ways, either:

(1) the addition of the Al_2O_3 in some way prevents the Si-clusters from forming; or, (2) the addition of the Al_2O_3 accelerates the formation of the clusters to such an extent that some (in the case of the 10 vol% Al_2O_3 composite) or all (in the case of the 15 vol% Al_2O_3 composite) of the Si-clusters form during quenching. A liquid nitrogen quench was also tried on the 15 vol% Al_2O_3 composite material, in an attempt to get a Si-cluster formation peak. The attempt was unsuccessful. Figure 8 shows a TEM bright field micrograph of the solutionized and as-quenched 6061Al - 15 vol% Al_2O_3 MMC. A high density of tiny Si-clusters is observed, thereby confirming that the Si-clusters form during quenching.

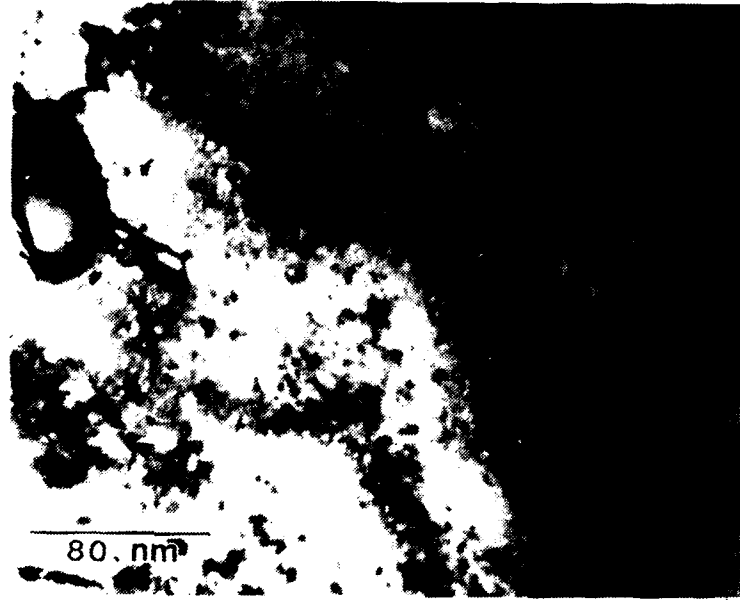


Figure 8: TEM micrograph (BF) of solutionized and as-quenched 15 vol% Al_2O_3 MMC showing a high density of tiny Si-clusters.

Second, although the Si-cluster peak in the 10 vol% Al_2O_3 is smaller than the peak for the monolithic alloy, the peak temperature (T_p) remains essential the same, i.e., T_p is approximately 355K.

Third, while the maximum of the convoluted GP-I/GP-II peak for the monolithic alloy appears to favor the GP-II peak, this peak in both of the composite samples appears to favor the GP-I peak. This would indicate that the addition of the alumina enhances the formation of the GP-I zones.

Finally, the size of the β -Mg₂Si peak decreases with increasing alumina content. This would indicate that the presence of alumina particle reinforcements stabilizes the intermediate phases, so that less of the equilibrium phase can form during the DSC scan.

Table II summarizes the temperatures of each peak (T_p) for the monolithic alloy and the two MMCs. It is evident from Table II that the formation of β' and β are accelerated with increasing reinforcement content.

Table II: Peak Temperature			
T_p	0 % Al ₂ O ₃	10 % Al ₂ O ₃	15 % Al ₂ O ₃
Si Clusters	355	355	-
GP-I	?	?	?
GP-II/ β''	?	?	?
β'	567	565	565
β	767	760	755

3. Effect of Pre-aging on the Precipitation of the Metastable Phases

Figure 9a shows the initial part of the DSC thermograms of the solutionized and as-quenched sample as well as the pre-aged samples of the monolithic 6061 alloy. Figure 9b shows the same thermograms for the 10 vol% Al_2O_3 composite material. Two features of these figures are noteworthy.

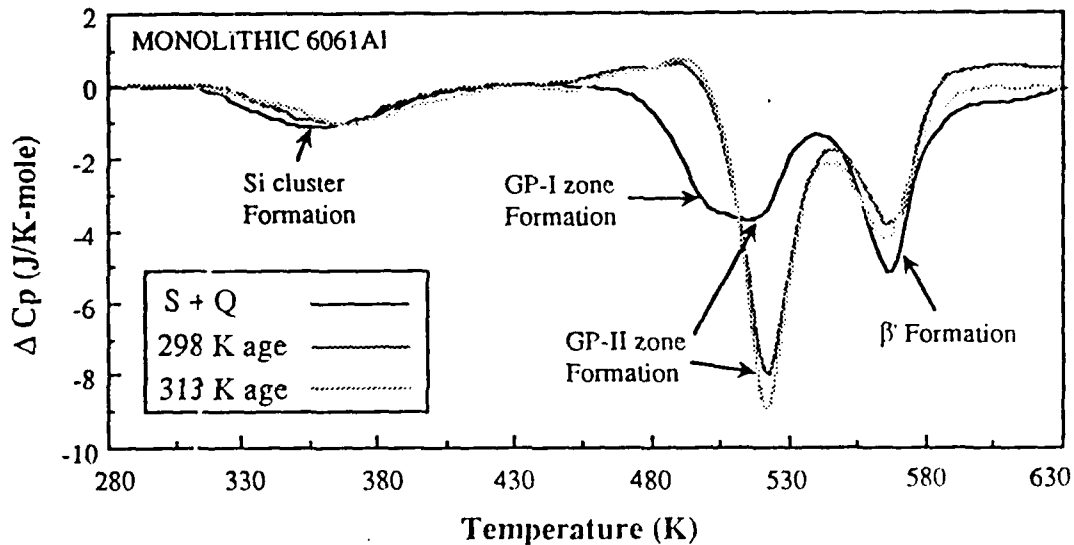


Figure 9a: DSC thermograms of the 6061Al alloy with no pre-aging and with pre-aging for 90 minutes at 25°C and 40°C.

First, the Si-cluster formation exotherm shifts to higher temperatures with increasing pre-aging temperatures, due to the increase in activation energy (E_a) for the precipitation of Si, as shown in Table III. This increase in E_a results in a concurrent increase in the activation free energy (ΔG). The explanation for the increasing activation energy is based on the vacancy-cluster mechanism proposed by Ozawa and Kimura [Ref. 11]. The pre-aging treatment reduces the number of the vacancy loops due to the coalescence and growth of the loops; therefore, the

number of Si-cluster nucleation sites is reduced. This increases the activation energy, since now energy must be expended to nucleate, as well as grow the Si-clusters.

Second, pre-aging seems to cause the disappearance of the GP-I zone formation peak, while enlarging the GP-II zone (β'') exotherm. This indicates that pre-aging supports the formation of GP-II zones directly from the Si-clusters without going through the intermediate GP-I zone. This result suggests that the formations of GP-I and GP-II zones from Si-clusters are parallel, competitive processes and not sequential events. If they were sequential events, the disappearance of the GP-I zone would be expected only if the peak due to Si-clustering were also absent. Figures 9a and 9b show that this is not the case.

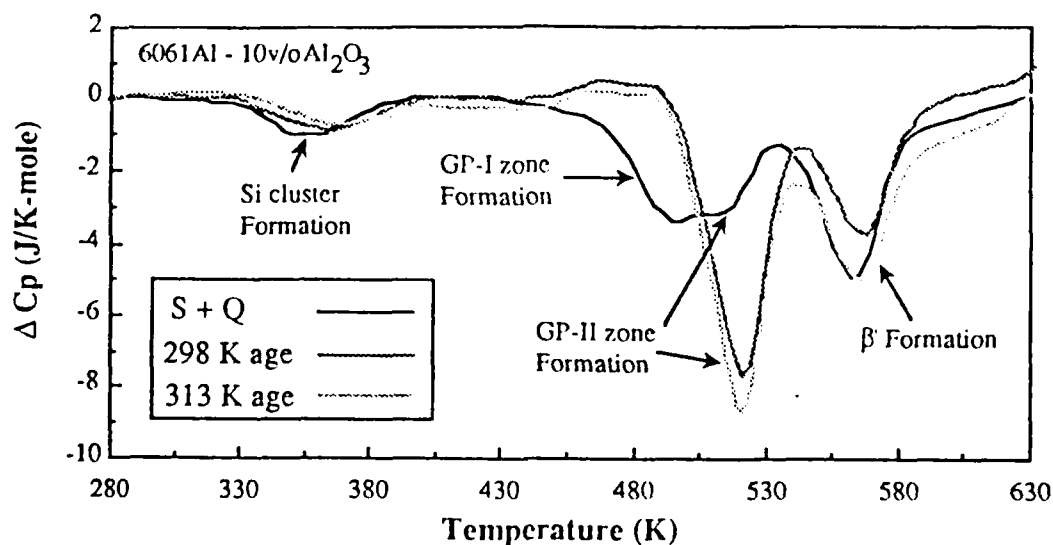


Figure 9b: DSC thermograms of the 10 vol% Al₂O₃ composite with no pre-aging, and with 90 minutes of pre-aging at 25°C and 40°C.

As seen in Table III, the heat of reaction, H_R , for the solutionized and as-quenched Al 6061-10 vol% Al_2O_3 is smaller than the heat of reaction for the

Table III: Summary of DSC Data						
Sample	T_p	H_R	E_a	ΔH	ΔS	ΔG
	K	J/mole	J/mole	J/mole	J/K-mole	J/mole
6061 No Aging	357	63.0	33095.0 ± 7594.2	30143.5 ± 7848.7	-204.0 ± 21.1	103083.0 ± 6212.8
6061 25°C Aging	362.5	57.9	43732.4 ± 21403.4	40739.4 ± 21598.5	-173.7 ± 60.5	104402.2 ± 4005.3
6061 40°C Aging	364.5	49.5	46445.6 ± 13166.5	43431.8 ± 13395.0	-172.0 ± 43.5	105183.5 ± 4627.5
6061 50°C Aging	368.9	26.6	51837.5 ± 19669.8	48823.7 ± 19899.9	-114.2 ± 65.3	105946.3 ± 4286.7
10 vol% No Aging	355	42.9	54625.9 ± 12039.8	51674.4 ± 12193.9	-143.2 ± 33.5	102655.7 ± 2505.7
10 vol% 25°C Aging	365	39.1	57656.9 ± 14363.3	54622.3 ± 14516.4	-135.8 ± 40.3	104798.3 ± 2689.4
10 vol% 40°C Aging	366.8	22.6	64491.0 ± 15626.0	61414.9 ± 15751.2	-116.9 ± 42.3	105176.1 ± 1869.9
10 vol% 50°C Aging	376	10.9	67667.2 ± 16273.4	64549.3 ± 16380.1	-112.5 ± 44.2	107176.7 ± 1604.7

solutionized and as-quenched monolithic alloy; and in both samples, H_R decreases as the pre-aging temperature increases. This indicates that a smaller volume

fraction of Si-clusters forms during the DSC scan, since the heat of reaction is proportional to the volume fraction of precipitates. As stated earlier, the concurrent increase in the peak temperature happens because of the reduction in the number of vacancy loops during pre-aging, leading to a reduction of the number of nucleation sites available. Since the same trend is observed in the composite, it can be inferred that a substantial fraction of the nucleation in the MMC occurs on the quenched-in vacancy loops, although the matrix dislocations also contribute to the nucleation process. If only the matrix dislocations were responsible for nucleation in the MMC, the observed rise in peak temperature due to the gradual annihilation of vacancy loops (nucleation sites) would not have occurred in the composite.

The smaller H_R for the solutionized and as-quenched composite material relative to the monolith is due to the fact that some Si-clusters in the MMC formed during the quench, leaving a smaller volume fraction available to be formed during the DSC scan. Assuming that the MMC and the monolith had approximately equal vacancy loop densities on quenching, then the acceleration in the nucleation of Si in the MMC must have occurred due to the presence of matrix dislocations, which act as sites for early nucleation. Therefore, it is inferred that during quenching, Si clustering occurs at the matrix dislocations which are already present. During aging, further clustering occurs in the quenched-in vacancy loops.

The decreasing H_R with increasing pre-aging temperature has essentially been explained by other researchers [Refs. 8, 12 and 14] and is based on the vacancy-cluster mechanism. In essence, as the pre-aging temperature increases, the

number of vacancy loops decreases. This reduces the number of Si-cluster nucleation sites and, since the diffusion of Si in the temperature range of the peak is fairly low, leads to a smaller volume fraction of clusters being formed.

The solutionized and as-quenched values for E_a and ΔH for the composite material are more than 65% higher than the same values for the monolithic alloy. The solutionized and as-quenched value for ΔS for the composite material is approximately 30% higher than the same value for the monolithic alloy; while there is an insignificant difference (less than 0.5%) between the solutionized and as-quenched value of ΔG for the composite material and the same value for the monolithic alloy. The higher activation energy (E_a) and hence the higher activation enthalpy (ΔH) in the solutionized and as-quenched composite is due to the fact that the Si-clusters form on the matrix dislocations during quenching, thereby deplete the matrix of solute atoms. Then, during the subsequent DSC scan, solute atoms must diffuse across longer distances in order to form Si-clusters on the quenched-in vacancy loops, leading to an increase in the activation energy. Since ΔH and E_a are related by the term RT , which is constant at the temperature of interest, the rise in E_a leads to a rise in ΔH . This increase in ΔH is balanced by a decrease in the magnitude of ΔS ; therefore, there is essentially no change in the activation free energy ΔG . The negligible difference between the free energy of Si clustering in the monolith and the MMC is responsible for the negligible difference between the Si-cluster formation peak temperatures in the monolith and the 10 vol% Al_2O_3 reinforced MMC.

While all four thermodynamic quantities, E_a , ΔH , ΔS , and ΔG , increase with increasing pre-aging temperature, for both the monolithic alloy and the composite material, the activation energy, E_a , and the activation enthalpy, ΔH , increase at a much faster rate for the monolithic alloy than for the composite material, e.g., the percent increase from the solutionized and as-quenched E_a to the 40°C pre-aged E_a is approximately 40%; the percent increase between the same two E_a 's for the composite material is only about 18%. The activation entropy, ΔS , shows a moderate rise (less than 20%); while, the free energy of formation ΔG shows only a small rise (approximately 2%) for both the monolithic alloy and the composite material.

The explanation for the increasing activation energy and activation enthalpy is also based on the vacancy-cluster mechanism. The pre-aging treatment annihilates some of the vacancy loops, therefore reducing the number of Si-cluster nucleation sites. This increases the activation energy, since now energy must be expended to nucleate, as well as grow the Si-clusters. But, since there is a high dislocation density in the composite material, the annihilation of some vacancy loops will have a lesser effect in the composite material than in the monolithic alloy because there will still be sufficient dislocations to act as preferential Si-cluster nucleation sites. Also, since dislocations can act as short-circuit paths for diffusion, the high dislocation density in the matrix of the composite assists the growth of existing Si-clusters.

C. RESISTIVITY

The results of the *in situ* resistivity measurements for the 10 vol% Al_2O_3 composite were combined with the data obtained by Hafley [Ref. 24] for the monolithic alloy and the 15 vol% Al_2O_3 composite and are presented in Figures 10 through 13. Figure 10 plots the results of the experiments conducted at an isothermal aging temperature of 200°C. This figure indicates that the resistivity

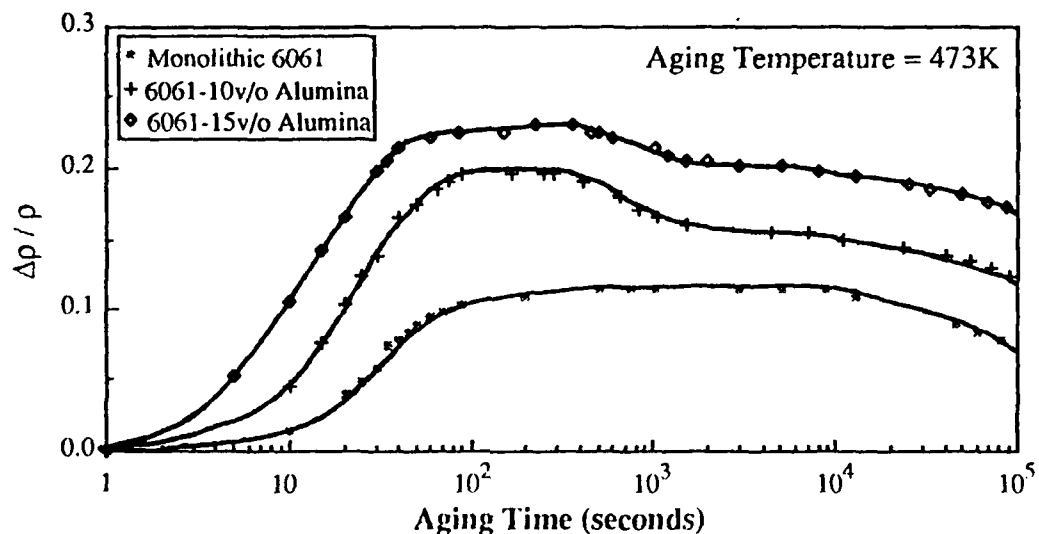


Figure 10: Changes in resistivity of 6061Al alloy reinforced with 0, 10 and 15 vol% Al_2O_3 , as a function of time at 200°C.

changes accompanying aging can be broadly divided into three zones:

- Zone I is the initial phase of aging characterized by the rapid increase in resistivity with respect to time.
- Zone II is the intermediate (peak) phase of aging characterized by the relatively flat region of zero resistivity change with respect to time.
- Zone III is final (overaged) phase of aging characterized by the slow decrease in resistivity with respect to time.

Zone I is related to the almost instantaneous nucleation and growth of Si-clusters, followed by the growth of the GP-I zones. Since these precipitates are completely coherent with the matrix, the stress field around the precipitates grows as the precipitates grow. This higher stress field impedes the flow of electrons more than removal of solute atoms from the solid solution can assist it. Therefore, there is a rapid rise in resistivity. Zone I covers about the same length of time for the monolithic alloy and the 10 vol% Al₂O₃ composite and is slightly shorter for the 15 vol% Al₂O₃ composite. However, the slopes of the two composite curves appear to be essentially the same; and they are significantly greater than the slope of the monolithic alloy. This indicates that the growth of Si-clusters and GP-I zones is accelerated in the composites. The peak value of $\Delta\rho/\rho$ increases with increasing Al₂O₃ content due to the increased matrix dislocation density.

Zone II is associated with the growth of the needle-like transition phases β'' and β' and is significantly shorter for both the composite materials, ending at approximately 500 seconds. For the monolithic alloy, however, Zone II does not end until approximately 10000 seconds. Since these needle-like precipitates are only partially coherent with the matrix, the stress fields around them are not as extensive. Therefore, the increase in resistivity associated with the growth of these phases is exactly balanced by the decrease in resistivity associated with the removal of the solute atoms from solid solution, so that there is a zero net change in resistivity of the material for the duration of Zone II. The accelerated growth of these transition phases was confirmed by the TEM study of the 15 vol% Al₂O₃ aged

at 473K for 315 seconds. At this aging treatment, the microstructure showed long coarse rods of the β' phase. In Hafley's work [Ref. 24], TEM micrographs of the monolithic alloy, after aging for 3000 seconds at 473K, showed that the microstructure still consisted primarily of very small needles and only a few rods. This indicates that, at 473K, the monolith is only starting to transform to β' after 3000 seconds, while the 15 vol% Al_2O_3 composite is ending this phase after only about 315 seconds.

Zone III covers the remainder of the test duration and is associated with the coarsening of the β' (rod-shaped) precipitate and the formation of the equilibrium β - Mg_2Si (plate-shaped) precipitate. Again, the result of Hafley's work [Ref. 24] confirms the presence of the incoherent β phase in the monolith after aging for 16 hours at 473K. The reduction in the net resistivity associated with this zone is due to the fact that both the stress field around the precipitates as the incoherent phase is formed and the number of solute atoms in solid solution are decreasing.

Figure 11 shows the results of the experiments conducted at an isothermal aging temperature of 373K. At this aging temperature, the initial rise in resistivity is associated with the growth of vacancy loops and the nucleation and growth of vacancy-Si-clusters. The TEM investigation conducted by Hafley [Ref. 24] of a monolithic sample aged for 100 second at 373K confirms the presence of a high density of small dislocation loops, some of which are decorated with very small precipitates. At 1200 seconds of aging, the TEM micrographs of the monolith show that the matrix is densely populated with very small precipitates. Hafley, identified

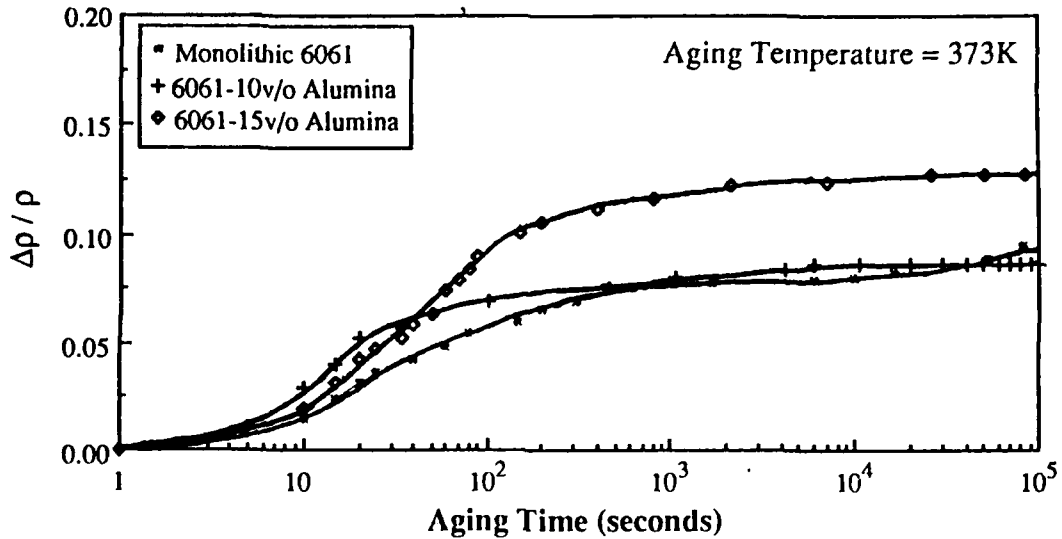


Figure 1: Changes in resistivity of 6061 Al reinforced with 0, 10, and 15 vol% Al_2O_3 , as a function of time at 100°C.

these precipitates as Si-clusters, although some GP-I zones may also be present. This is based on the fact that the resistivity curve is just beginning to level out in the monolith. In the composites, the vacancy-Si-clusters will nucleate and grow very rapidly, as evidenced by the rapid rise in resistivity. Therefore, for most of the duration of this test, the resistivity changes in the composites are associated mainly with the growth of the GP-I zones.

Figure 12 plots the results of the resistivity measurements conducted at an isothermal aging temperature of 323K. For the duration of this test, the resistivity of all three materials continues to rise, but the microstructural changes associated with this rise is considered to be different in all three materials. This consideration is based on the fact that the diffusion rate of Si at this temperature is relatively slow and that there are already Si-clusters present in the composites due to the

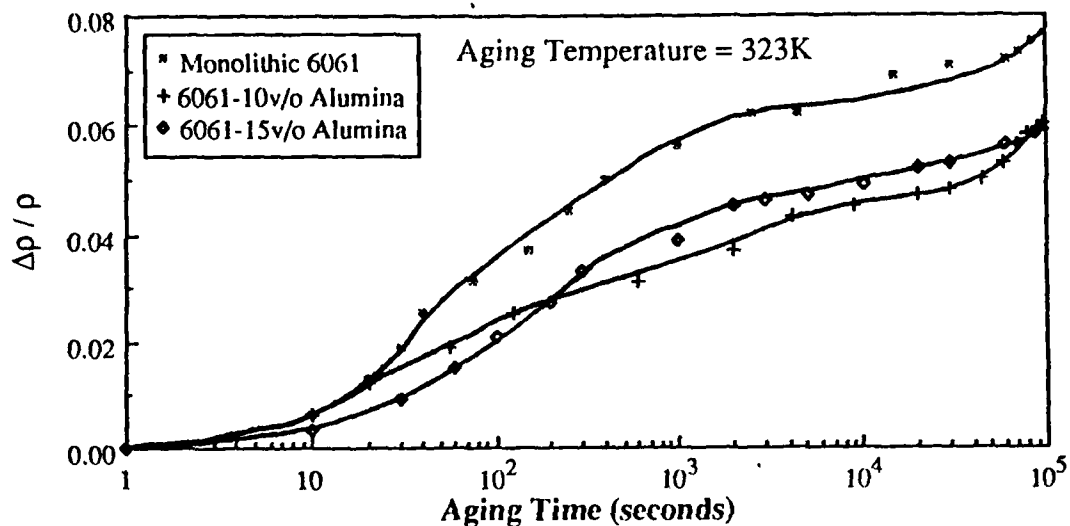


Figure 12: Changes in resistivity of 6061Al reinforced with 0, 10 and 15 vol% Al_2O_3 , as a function of time at 50°C.

precipitation which occurred on the matrix dislocations during quenching. In the monolith the rise in resistivity is thought to be due to the nucleation and growth of Si-clusters. In the 10 vol% Al_2O_3 composite, the rise is attributed to the growth of Si-clusters and GP-I zones and in the 15 vol% Al_2O_3 composite, the rise is attributed to the growth of GP-I zones.

Figure 13 shows the results of the experiments conducted at room temperature. The figure shows that is essentially no changes in resistivity in any of the materials for the first 1000 seconds. At that time the 10 vol% Al_2O_3 composite begins to show a rapid rise in resistivity, followed by a more gradual, but still increasing change. The monolithic alloy shows a similar trend, but the start is delayed until about 5000 seconds. The 15 vol% Al_2O_3 never shows any change in resistivity.

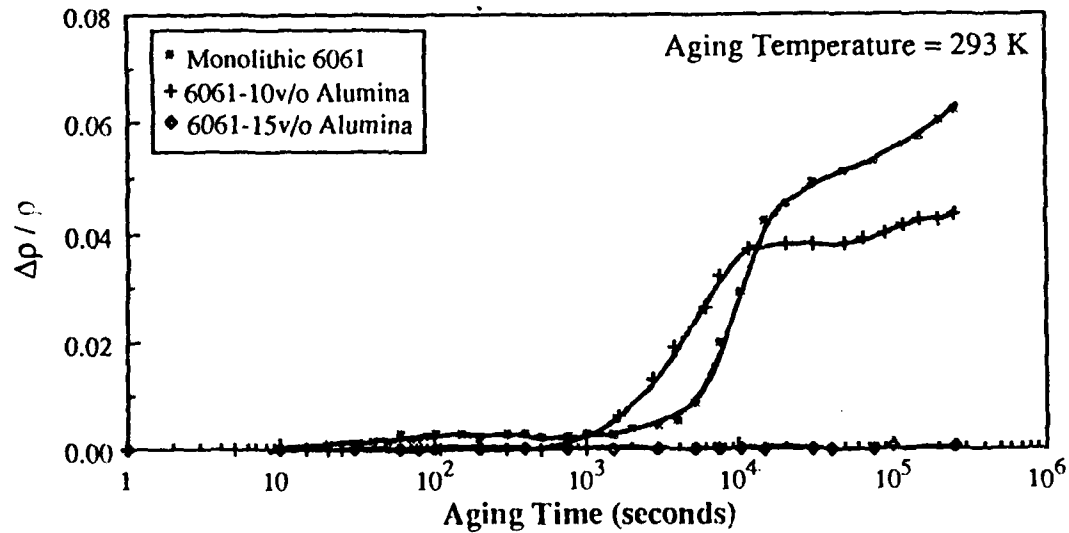


Figure 13: Changes in resistivity of 6061Al alloy reinforced with 0, 10 and 15 vol% Al_2O_3 , as a function of time at 20°C.

Comparison of these results with the DSC results would indicate that the initial rapid rise in resistivity is associated with the nucleation and growth of Si-clusters. This would explain why there is no change in resistivity in the 15 vol% Al_2O_3 composite; the Si-clusters were already formed on the matrix dislocations during quenching. The amount of time (3 days) at this temperature was insufficient for the precipitation of the GP-I zones to begin. The monolithic alloy and the 10 vol% Al_2O_3 composite show the typical S-shaped curve associated with a diffusional nucleation and growth process. The initial rapid rise in resistivity is associated with the nucleation dominated phase of the precipitation process. The inflection in the two curves indicated the point at the precipitation process changes from nucleation dominated to growth dominated.

V. CONCLUSIONS

The addition of as little as 10 vol% Al_2O_3 does accelerate the aging process of 6061Al; the effects are even greater with higher alumina content. This is most easily seen in the hardness results, where the time to peak hardness at 200°C decreases from approximately 70 minutes in the monolith to approximately 40 minutes in the 10 vol% alumina composite. The time to peak hardness decreases even further to approximately 20 minutes in the 15 vol% composite.

Differential scanning calorimetry coupled with TEM observations and resistivity measurements reveal that both nucleation and growth are accelerated in the composite. Nucleation of Si-clusters occurs during quenching on the punched-out *dislocations in the matrix* of the composites, as seen both in the decrease in size of the Si-cluster formation peak with increasing alumina reinforcements and in the TEM observation of the solutionized and as-quenched 15 vol% Al_2O_3 composite. The nucleation of Si-clusters on the quenched-in vacancy loops, which occurs during subsequent aging is not accelerated, since the peak temperature of the Si-cluster formation peak does not change with increasing reinforcement. The decrease in the peak temperatures of the transition precipitates suggests that the growth of these phases is accelerated. This conclusion can also be drawn from the resistivity results, since the horizontal portion of the resistivity curves, which is associated with the growth of the needle-like transition phases is significantly shorter in the composites.

Finally, the accelerated growth is confirmed by the TEM observations associated with the resistivity measurements.

The presence of reinforcements stabilizes the transition phases and suppresses the formation of the β phase, as indicated by the decrease in the size of the equilibrium β -Mg₂Si formation peak with increasing alumina content. The presence of reinforcements also enhances the formation of GP-I zones.

Pre-aging has the same effects on the composite and monolithic materials which are: (1) to increase the Si-cluster formation peak temperatures with increasing pre-aging temperatures due to the increase in activation energy ; and (2) to enhance the GP-II zone formation indicating that the formation of the GP zones are competitive vice sequential in nature.

LIST OF REFERENCES

1. Hunt, M., "Aluminum Composites Come of Age", Materials Engineering, Vol.106, pp 37-40, January 1989.
2. Rohatgi, P., "Advances in Cast MMCs", Advanced Materials and Processes, Vol. 137, Issue 2, pp 39-44, February, 1990.
3. Abkowitz, S. and Weihrauch, P., "Trimming the Cost of MMCs", Advanced Materials and Processes, Vol. 136, Issue 1, pp. 31-34, July 1989.
4. Hoover, W. R., "Castable MMCs: A new alternative", Advanced Materials and Processes, Vol. 137, Issue 2, p. 42, February 1990.
5. DeMeis, R., "New Life for Aluminum", Aerospace America, Vol. 27, No. 3, pp 26-29, March 1989.
6. Parker, E. R., Material Data Book for Engineers and Scientists, McGraw-Hill Book Co., p. 70, 1967.
7. Lutts, A., "Pre-Precipitation in Al-Mg-Ge and Al-Mg-Si", Acta Metallurgica, Vol. 9, pp. 577-586, June 1961.
8. Thomas, G., "The Aging Characteristics of Aluminium Alloys", Journal of the Institute of Metals, Vol. 90, pp. 57-63, 1961-62.
9. Cordier, H. and Gruhl, W., "Beitrag zur Frage der Entmischung bei AlMgSi-Legierungen aufgrund elektronenmikroskopischer Beobachtungen", Zeitschrift für Metallkunde, Vol. 56, pp. 669-674, 1965.
10. Ceresara, S., Di Russo, E., Fiorini, P., and Giarda, A., "Effect of Si Excess on the Aging Behavior of Al-Mg₂Si 0.8% Alloy", Material Science and Engineering, Vol. 5, pp. 220-227, 1960/70.
11. Ozawa, E. and Kimura, H., "Excess Vacancies and the Nucleation of Precipitates in Aluminum-Silicon Alloys", Acta Metallurgica, Vol. 18, pp. 995-1004, September 1970.

12. Kovacs, I., Lendvai, J., and Nagy, E., "The Mechanism of Clustering in Supersaturated Solid Solutions of Al-Mg₂Si Alloys", Acta Metallurgica, Vol. 20, pp. 975-983, July 1972.
13. Smith, W. F., "The Effect of Reversion Treatments on Precipitation Mechanisms in an Al-1.35 at. pct Mg₂Si Alloy", Metallurgical Transactions, Vol. 4, pp. 2435-2440, October 1973.
14. Lendvai, J., Ungar, T., and Kovacs, I., "The Effect of the Temperature of Solution Treatment and Quenching on the Zone Formation Process in Al-Mg-Si Alloys", Materials Science and Engineering. Vol. 16, pp. 85-89, 1974.
15. Rack, H. J. and Krenzer, R. W., "Thermomechanical Treatment of High Purity 6061 Aluminum", Metallurgical Transactions A, Vol. 8A, pp. 335-346, February 1977.
16. Nieh, T. G. and Karlak, R. F., "Aging Characteristics of B₄C-Reinforced 6061-Aluminum", Scripta Metallurgica, Vol. 18, No. 1, p. 25, 1984.
17. Dutta, I., Bourell, D. L. and Latimer, D., "A Theoretical Investigation of Accelerated Aging in Metal-Matrix Composites", Journal of Composite Materials, Vol. 22, pp. 829-849, September, 1988.
18. Christman, T. and Suresh, S., "Microstructural Development in an Aluminum Alloy-SiC Whisker Composite", Acta Metallurgica, Vol. 36, No. 7, pp 1691-1704, 1988.
19. Dutta, I. and Bourell, D. L., "A Theoretical and Experimental Study of Aluminum Alloy 6061-SiC Metal Matrix Composite to Identify the Operative Mechanism for Accelerated Aging", Materials Science and Engineering, Vol. A112, pp. 67-77, 1989.
20. Vogelsang, M., Arsenault, R. J., and Fisher, R. M., "An *In Situ* HVEM Study of Dislocation Generation at Al/SiC Interfaces in Metal Matrix Composites", Metallurgical Transactions A, Vol. 17A, pp. 379-389, March 1986.
21. Papazian, J. M., "Effects of SiC Whiskers and Particles on Precipitation in Aluminum Matrix Composites", Metallurgical Transactions A, Vol. 19A, pp. 2945-2953, December 1988.
22. Suresh, S., Christman, T. and Sugimura, Y., "Accelerated Aging in Cast Al Alloy-SiC Particulate Composites", Scripta Metallurgica, Vol. 23, pp. 1599-1602, 1989.

23. Arsenault, R. J. and Fisher, R. M., "Microstructure of Fiber and Particulate SiC in 6061 Al Composites", Scripta Metallurgica, Vol. 17, pp. 67-71, 1983.
24. Hafley, J. L., "A Comparison of the Aging Kinetics of a Cast Alumina-6061 Aluminum Composite and a Monolithic 6061 Aluminum Alloy", Master's Thesis, Naval Postgraduate School, Monterey, California, December 1989.
25. Frost, A. A. and Pearson, R. G., Kinetics and Mechanisms, pp. 77-102, J. Wiley and Sons, Inc., 1961.
26. Adler, P. N. and Delasi, R., "Calorimetric Studies of 7000 Series Aluminum Alloys: II. Comparison of 7075, 7050 and RX720 Alloys", Metallurgical Transactions A, Vol. 8A, pp. 1185-1190, July 1977.
27. Osamura K. and Ogura, T., "Metastable Phases in the Early Stage of Precipitation in Al-Mg Alloys", Metallurgical Transactions A, Vol. 15A, pp. 835-842, May 1984.
28. Pashley, D. W., Rhodes, J. W. and Sendorek, A., "Delayed Ageing in Aluminium-Magnesium-Silicon Alloys: Effect on Structure and Mechanical Properties", Journal of the Institute of Metals, Vol. 94, pp. 41-49, 1966.
29. Jacobs, M. H., "The Structure of the Metastable Precipitates Formed During Ageing of an Al-Mg-Si Alloy", The Philosophical Magazine, Vol. 26, pp. 2-13, 1972.